Tan, R. K. Z., & Harvey, S. C. (1989) *J. Mol. Biol. 205*, 573–592.
van der Ploeg, P., & Berendsen, H. J. C. (1982) *J. Chem. Phys. 76*, 3271–3276.
van der Ploeg, P., & Berendsen, H. J. C. (1983) *Mol. Phys. 49*, 233–248.
Verlet, L. (1967) *Phys. Rev. 159*, 98.
Watanabe, K., Ferrario, M., & Klein, M. (1988) *J. Phys. Chem. 92*, 818–821.
Weiner, S. J., Kollman, P. A., Case, D. A., Singh, U. C., Ghio, C., Alagona, G., Profeta, S., & Weiner, P. (1984) *J. Am. Chem. Soc. 106*, 765–784.
Wendoloski, I. J., Kimatian, S. J., Schutt, C. E., & Salemme, F. R. (1989) *Science 243*, 637–638.
Zaccai, G., Buldt, G., Seelig, A., & Seelig, J. (1979) *J. Mol. Biol. 134*, 693–706.
Zwanzig, R., & Ailawadi, N. K. (1969) *Phys. Rev. 182*, 280–284.

Frequency-Domain Fluorescence Spectroscopy Resolves the Location of Maleimide-Directed Spectroscopic Probes within the Tertiary Structure of the Ca-ATPase of Sarcoplasmic Reticulum†

Diana J. Bigelow* and Giuseppe Inesi
Department of Biological Chemistry, University of Maryland School of Medicine, 660 West Redwood Street, Baltimore, Maryland 21201

Received July 17, 1990; Revised Manuscript Received November 14, 1990

ABSTRACT: We have used fluorescence spectroscopy to characterize three covalently bound spectroscopic maleimide derivatives with respect to their location within the tertiary structure of the Ca-ATPase of sarcoplasmic reticulum (SR). These derivatives include (1) 2-(4′-maleimidoanilino)naphthalene-6-sulfonic acid, (2) 4-(dimethylamino)azobenzene-4′-maleimide, and (3) fluorescein 5′-maleimide. Biochemical assays demonstrate that modification with any of these three derivatives results in the same functional effects, observed following derivatization of cysteines 344 and 364 by *N*-ethylmaleimide [Saito-Nakatsuka et al. (1987) *J. Biochem. (Tokyo) 101*, 365–376]. These residues bracket the ATPase's phosphorylation site (Asp 351) and thus may provide spectroscopic probes of the protein's conformation in this essential region. In agreement with sequencing results, SDS–polyacrylamide gels show that maleimide-modified SR exhibits fluorescence exclusively on the A_1 tryptic fragment of the Ca-ATPase. Extensive tryptic digestion followed by centrifugation demonstrates essentially all of the fluorescence was associated with the soluble rather than insoluble (membrane-associated) peptides, confirming the predicted extramembraneous location of these residues. Utilizing frequency-domain fluorescence spectroscopy, we were able to recover the transient effects associated with a distribution of donor–acceptor distances. We find from these fluorescence resonance energy transfer measurements that covalently bound maleimide probes are 36 Å apart, independent of whether a discrete distance is assumed or a distance distribution model is utilized, in which the conformational variability of the protein is taken into account. While a unimodal distance distribution is adequate to describe the intensity decay associated with maleimide-directed donor–acceptor pairs, a bimodal distribution of distances is necessary to describe the frequency response associated with the energy transfer between maleimide-directed chromophores and other covalently bound probes on the Ca-ATPase, consistent with the large spatial separation observed between maleimides. We recover mean distances of 42 and 77 Å between maleimide sites and bound FITC (Lys 515) and mean distances of 28 and 37 Å between the maleimide- and the iodoacetamide-directed probes (Cys 670 and 674, whose close proximity approximates a single locus). The measured distances are presented in a model and have permitted us to describe a unique arrangement of these covalently bound probes within both the secondary and tertiary structure of the Ca-ATPase. The resolution inherent in the frequency-domain fluorescence technique to multiple donor–acceptor distances should be generally applicable to a wide range of biological systems in which specific labeling of single unique donor–acceptor sites is not feasible.

Reactive cysteines of the Ca-ATPase of sarcoplasmic reticulum (SR)[1] have often been effectively utilized as convenient sites of attachment for spectroscopic probes, allowing the elucidation of many of the protein's structural features and conformational changes (Champeil et al., 1976; Coan & Inesi, 1977; Hidalgo et al., 1978; Thomas & Hidalgo, 1978; Coan et al., 1979; Guillain et al., 1981; Miki et al., 1981; Yasuoka-Yabe & Kawakita, 1983; Bigelow et al., 1984; Bigelow & Thomas, 1987; Squier et al., 1988). Iodoacetamide and maleimide derivatives have frequently been used due to the dif-

† Supported by NHBLI (PO1 HL27867).
* To whom correspondence should be addressed at the Department of Biochemistry, The University of Kansas, Haworth Hall, Lawrence, KS 66045-2106.

[1] Abbreviations: SR, sarcoplasmic reticulum; NEM, *N*-ethylmaleimide; ANSmal, 2-(4′-maleimidoanilino)naphthalene-6-sulfonic acid; DABmal, 4-(dimethylamino)azobenzene-4′-maleimide; Fmal, fluorescein 5′-maleimide; FITC, fluorescein 5′-isothiocyanate; IAEDANS, 5-[[2-[(iodoacetyl)amino]ethyl]amino]naphthalene-1-sulfonic acid; IAF, 5-(iodoacetamido)fluorescein.

0006-2960/91/0430-2113$02.50/0

ferential reactivity of the ATPase's sulfhydryls, at neutral pH, toward these reagents (Hasselbach & Seraydarian, 1966; Yoshida & Tonomura, 1976; Thorley-Lawson & Green, 1977; Murphy, 1978; Yamada & Ikemoto, 1978). Several maleimide-directed probes have been found to label the Ca-ATPase with a different specificity than iodoacetamide-directed probes (Bishop et al., 1988; Saito-Nakatsuka et al., 1987), allowing the selective modification of different cysteinyl side chains.

The amino acid residues modified by fluorescent iodoacetamides have been identified when derivatized under several conditions (Yamashita & Kawakita, 1987; Suzuki et al., 1987; Bishop et al., 1988). These residues (cysteines 670 and 674) can be modified without loss of transport activity and are located in the cytoplasmic portion of the B tryptic domain (Squier et al., 1987). Moreover, these sites have been estimated from fluorescence resonance energy transfer to be *distant* (relative to the native protein's overall dimensions) from fluorescein isothiocyanate (FITC) covalently bound at the nucleotide site and *close* to lanthanides that may be bound near the high-affinity calcium binding sites (Squier et al., 1987). While these iodoacetamide probes label multiple sites, their close proximity within the primary sequence assures that, to a good approximation, they serve as an effective site that in conjunction with fluorescence resonance energy transfer can be utilized in the determination of the distance between this site and other specifically modified residues, where a unique distance of separation between donor and acceptor fluorophores is generally assumed.

Like the iodoacetamide-modified sites, two amino acid residues, i.e., cysteines 344 and 364, have been found to be highly reactive to chemical modification by *N*-ethylmaleimide (NEM; Saito-Nakatsuka et al., 1987; Yamashita & Kawakita, 1987). The large separation between these residues within the primary sequence indicates that they cannot be assumed, a priori, to approximate a single site for fluorescence energy transfer studies. However, the labeling of these sites occurs with negative cooperativity, such that the first label randomly binds to either cysteine 344 or 364, retarding the covalent attachment of the second label to each ATPase molecule (Saito-Nakatsuka et al., 1987). This property has allowed us to utilize maleimide-directed probes containing different chromophoric groups (with the appropriate spectral properties) to measure the effective distance of separation between these important amino acids, which bracket the phosphorylation site (Asp 351) on the Ca-ATPase, and in this way to monitor the conformation of this polypeptide segment that may play an important role in the formation and hydrolysis of the phosphoenzyme and overall turnover of the ATPase.

Moreover, we were able to characterize the position of these labels within the tertiary structure of the ATPase, by measuring both (a) their sensitivity to collisional quenching and susceptibility to tryptic digestion and (b) their separation relative to other covalent probes bound to the cytoplasmic domain through the use of fluorescence resonance energy transfer. These probes include (1) FITC and (2) iodoacetamide-directed probes, either 5-(iodoacetamido)fluorescein (IAF) or 5-[[2-[(iodoacetyl)amino]ethyl]amino]-naphthalene-1-sulfonic acid (IAEDANS), as well as (3) the intrinsic tryptophans predicted to reside primarily within the membrane (Brandl et al., 1986). These results thus localize these maleimide probes and provide a greater understanding of the tertiary structure of the Ca-ATPase.

Experimental Procedures

Materials. 2-(4′-Maleimidoanilino)naphthalene-6-sulfonic acid (ANSmal), 4-(dimethylamino)azobenzene-4′-maleimide (DABmal), fluorescein 5′-maleimide (Fmal), and 5-(iodoacetamido)fluorescein (IAF) were purchased from Molecular Probes (Eugene, OR); fluorescein 5′-isothiocyanate (FITC) and 5-[[2-[(iodoacetyl)amino]ethyl]amino]naphthalene-1-sulfonic acid (IAEDANS) were obtained from Sigma Chemical Co. (St. Louis).

Biochemical Methods. Purified preparations of longitudinal sarcoplasmic reticulum ("light") vesicles were obtained from rabbit skeletal muscle as described by Saito et al. (1984). Detergent-solubilized vesicles were prepared by including 1 mg of 2-myristoyllysophosphatidylcholine (lysolecithin)/mg of SR protein in a buffer consisting of 20 mM MOPS (pH 6.8), 80 mM KCl, 5 mM $MgCl_2$, 0.5 mM EGTA, and 0.6 mM $CaCl_2$ (Ludi and Hasselbach, 1985). Previously it has been demonstrated that there is significant energy transfer between fluorescent probes covalently bound to different ATPase molecules in native SR membranes (Highsmith & Cohen, 1987; Bigelow et al., 1988). Therefore, this solubilized preparation was used for fluorescence resonance energy transfer measurements to ensure that fluorescence measurements reflected only energy transfer between probes on the same polypeptide chain. Rates of Ca-dependent ATPase activity from these preparations are equal to those of ionophore-treated native vesicles, demonstrating that the native conformation of the enzyme is maintained under these conditions. Protein concentrations were determined by the method of Lowry et al. (1951) or by absorbance, by using $\epsilon_{280} = 10.5$ cm^{-1} for 10 mg of SR protein/mL in 1% sodium dodecyl sulfate solution (Thorley-Lawson & Green, 1977). Limited tryptic cleavage, denaturing polyacrylamide gel electrophoresis (Weber & Osborne, 1969), and visualization of fluorescence on these gels were done as described previously (Squier et al., 1987). Extensive tryptic digestion was performed in a buffer consisting of 50 mM $(NH_4)HCO_3$ (pH 8.5), 100 μM $CaCl_2$, 2 mM DTT, and 5 mg of SR protein/mL, with a trypsin:SR protein ratio of 1:100, for 4 h at 37 °C. Subsequently, the preparation was centrifuged at 40000*g* for 60 min, the supernatant was decanted, the pellet was resuspended in a small volume of the above buffer, and each was assayed for probe and protein concentrations as described elsewhere under Experimental Procedures.

Functional Assays. Ca-dependent ATPase activity was measured by a colorimetric determination of inorganic phosphate released from vesicles made leaky to calcium by the addition of the ionophore A23187 (Lanzetta et al., 1979). Phosphoenzyme was formed from [^{32}P]ATP in a medium of 20 mM MOPS (pH 7.0), 5 mM $MgCl_2$, 1 mM EGTA, 80 mM KCl, 0.9 mM $CaCl_2$ and 0.5 mg of SR protein/mL; the reaction was started by addition of 0.1 mM [γ-^{32}P]ATP and, following a 20-s incubation at 25 °C, quenched with 3.5% (v/v) trichloroacetic acid. The quenched protein was washed four times by repeated centrifugations and resuspensions in 3.5% TCA, and the final sediment was dissolved in 1% SDS. The final samples were assayed for protein and ^{32}P.

Probe Labeling. The Ca-ATPase was labeled with ANSmal, Fmal, or DABmal essentially as described previously (Yasuoka-Yabe & Kawakita, 1983; Saito-Nakatsuka et al., 1987). The first step involved prelabeling the SR with NEM in order to block fast-reacting low molecular weight proteins in the preparation; this was accomplished in a labeling medium of 20 mM MOPS (pH 7.0), 5 mM $MgCl_2$, and 80 mM KCl with 50 mM NEM and a SR protein concentration of 10 mg/mL at 0 °C in the dark for 30 min. By using [^{3}H]NEM for this step, it was found that 1.2 (±0.2) nmol of NEM was incorporated/mg of SR protein with no effect on enzymatic

activity. The reaction medium was diluted in the above labeling buffer to a protein concentration of 3 mg/mL and allowed to equilibrate at 24 °C before the addition of the spectroscopic maleimide (from a 10 mM stock solution in dimethylformamide) to initiate labeling with this probe in the dark for 40 min. In handling maleimide derivatives, care was taken to avoid pH > 8.0, which promotes hydrolysis of the maleimide ring (Ishi & Lehrer, 1986). Unreacted probe was removed by using a Sephadex G-50 column followed by washing in an excess of buffer [0.3 M sucrose and 20 mM MOPS (pH 7.0)] and the labeled SR was concentrated by centrifugation (100000*g*) for 45 min. Preliminary experiments involving separation of labeled peptides on HPLC for amino acid sequencing revealed that the majority of the peaks corresponded to probe that was not associated with protein (Wawrzynow et al., 1990), which might be attributed to either (1) the hydrolytic instability of the maleimide ring under these conditions (Ishi & Lehrer, 1986) or (2) the presence of unreacted probe that was not removed from the protein sample. Several lines of evidence indicate that no significant fraction of unreacted probe is present in samples used for spectroscopic and functional studies: (1) Both steady-state and time-resolved anisotropy of Fmal- or ANSmal-derivatized SR preparations reveal restricted motion with no evidence for the presence of a mobile fraction characteristic of probe that is lipid-bound or free in solution. (2) The absorption spectrum of DABmal reacted with the SR is characterized by a dramatic blue shift (36 nm) relative to free DABmal. (3) Energy transfer measurements involving these probes indicate two specific sites (see Results) rather than multiple and random probe locations, as would be expected from noncovalent interactions with the protein. However, these preliminary results confirm that cysteine 364 is a major labeling site (Wawrzynow et al., 1990), in agreement with results obtained with NEM (Saito-Nakatsuka et al., 1987; Yamashita & Kawakita, 1987).

Modification of the Ca-ATPase with FITC, IAEDANS, and IAF was performed as described previously (Squier et al., 1987). The stoichiometry of labeling for the probes used in this study was measured in the presence of 1% sodium dodecyl sulfate and 0.1 M NaOH, with the following measured extinction coefficients: ϵ_{495}(FITC) = 8.0×10^4 M^{-1} cm^{-1} (Mitchinson et al., 1982); ϵ_{340}(IAEDANS) = 6100 M^{-1} cm^{-1}; ϵ_{495}(IAF) = 7.5×10^4 M^{-1} cm^{-1} (Eshaghpour et al., 1980); ϵ_{330}(ANSmal) = 2.0×10^4 M^{-1} cm^{-1}; ϵ_{495}(Fmal) = 7.8×10^4 M^{-1} cm^{-1}; and ϵ_{460}(DABmal) = 24.8×10^4 M^{-1} cm^{-1}.

Fluorescence Measurements. (*A*) *Steady-state fluorescence intensities* were obtained with an SLM 8000 fluorometer with excitation and emission monochromators. Polarization artifacts were eliminated by setting the emission polarizer at 54.7° relative to the excitation light.

Steady-state polarization (P) was calculated from the ratio of the fluorescence intensities (I) with the polarizers in the vertical (v) or horizontal (h) position:

$$P = (I_{vv} - GI_{vh})/(I_{vv} + GI_{vh}) \quad (1)$$

where $G = I_{hv}/I_{hh}$ and corrects for the differing sensitivities of the detection system for vertically and horizontally polarized light.

(*B*) *Frequency-domain data* were measured on a frequency-domain fluorometer described previously (Lakowicz et al., 1986a,b). The modulated excitation was provided by the harmonic content of a laser pulse train with a repetition rate of 3.79 MHz and a pulse width of 5 ps, from a synchronously pumped and cavity-dumped rhodamine 6 G or pyridine-2 dye laser. The dye laser was pumped with a mode-locked argon ion laser (Coherent, Innova 15). The rhodamine dye laser output was frequency-doubled with an angle-tuned KDP crystal to either 298 nm, for tryptophan excitation, or 307 nm, for ANSmal excitation; the pyridine dye laser was similarly frequency-doubled to 350 nm for IAEDANS excitation. The emitted light was observed with a microchannel photomultiplier, and the cross-correlation detection was performed outside the PMT. The emission was observed through a combination of broad-band and cutoff emission filters (see figure legends for experimental details). For intensity decay measurements, magic angle polarizer orientations were used.

The frequency-domain data were analyzed by the method of nonlinear least-squares (Gratton et al., 1984; Lakowicz et al., 1984). The measured data are compared with values predicted from a model, and the parameters of the model are varied to yield the minimum deviations from the data. For the case of a multiexponential decay, the impulse response $I(t)$ is given by

$$I(t) = \sum \alpha_i e^{-t/\tau_i} \quad (2)$$

where α_i is the preexponential factor and τ_i is the decay time.

Alternatively, the intensity decays can be modeled as a Gaussian distribution of decay times (Alcala et al., 1987; James et al., 1987; Lakowicz et al., 1987b).

Energy Transfer Measurements. The effect of appropriate acceptors (A) on the fluorescence intensity and lifetime of the donor (D) was used to measure the donor–acceptor distance from the efficiency of energy transfer (E):

$$E = 1 - \tau/\tau_0 = 1 - F/F_0 \quad (3)$$

τ_0 or F_0 refers to the lifetime or steady-state fluorescence yield, respectively, of the bound donor. When multiple lifetimes are observed, E can be calculated from

$$E = 1 - \sum(\alpha_i\tau_i)/\sum(\alpha_i\tau_i)_0 \quad (4)$$

where $(\alpha_i\tau_i)_0$ and $(\alpha_i\tau_i)$ are parameters that are proportional to the quantum yield (Luedtke et al., 1981), and refer to lifetime and amplitude in the absence and presence of energy transfer, respectively.

The efficiency of energy transfer is directly related to the distance between donor and acceptor (r) by

$$E = r^6/(r^6 + R_0^6) \quad (5)$$

R_0 is the (Forster) distance in angstroms where energy transfer is 50% and is given by

$$R_0 = (9.79 \times 10^3)(\kappa^2 n^{-4} QJ)^{1/6} \quad (6)$$

where κ^2 is the orientation factor, n is the refractive index, Q is the quantum yield of the donor in the absence of the acceptor, and J is the spectral overlap integral (Lakowicz, 1983; see Figure 1). Quantum yields, measured relative to the reference compound quinine bisulfate (Chen, 1974), are 0.20 for ANSmal–SR, 0.13 for intrinsic tryptophans, and 0.54 for IAEDANS–SR (Squier et al., 1987); these values are unaltered by the addition of the detergent lysolecithin (1 mg/mg of SR protein). The refractive index, n, has been taken for proteins to be 1.4. The calculated distances are somewhat uncertain depending upon the extent of static and dynamic averaging of the orientation factor (Dale et al., 1979; Dale & Eisinger, 1975). In our analysis we assume the value of κ^2 to be $^2/_3$ due to the range of conformations, the possibility of rotational diffusion, and the mixed polarization of the species (Haas et al., 1978). The use of $\kappa^2 = {}^2/_3$ is not likely to result in significant error if donor and acceptor can adopt a range of conformations (Englert & Leclerc, 1978).

Distance Distributions. We also used energy transfer to determine the distribution of distances between donor and

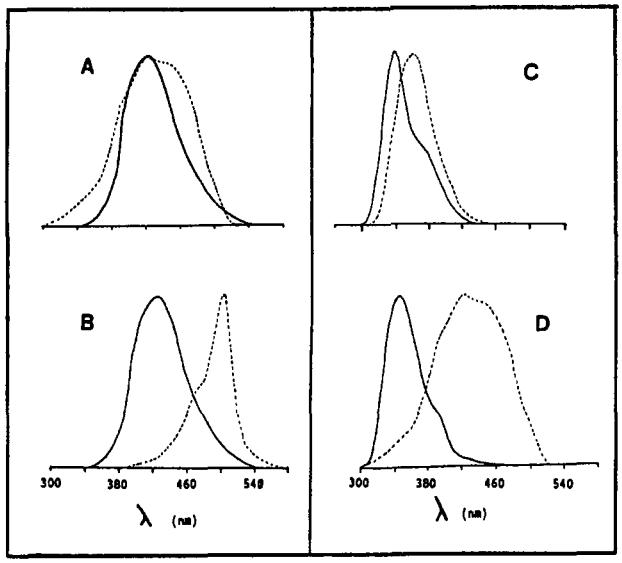

FIGURE 1: Spectral overlap between donor emission and acceptor absorption. Solid lines represent fluorescence emission spectra of ANSmal–SR (panels A and B) with excitation at 307 nm and of intrinsic tryptophans (panels C and D) with excitation at 298 nm. Dotted lines represent absorption spectra of DABmal–SR (panels A and D), FITC– or Fmal–SR (panel B), and ANSmal (panel C).

acceptors on the Ca-ATPase. The distance distribution was modeled either as a unimodal or bimodal Gaussian; pertinent equations are described elsewhere (Lakowicz et al., 1987a,b, 1988).

RESULTS

In order to localize the position of maleimide-directed probes within the tertiary structure of the Ca-ATPase, we have utilized three maleimide derivatives whose differing spectroscopic properties allow their use as either energy transfer donors or acceptors, thereby serving to minimize potential errors that may arise in the calculation of distances from a single donor–acceptor pair whose photophysical properties and orientational effects might skew the apparent distance (Dale & Eisinger, 1974). In addition, the use of a range of chromophores has allowed us to test an earlier proposal that the chromophoric moiety directs the specificity of a probe's reaction with amino acid side chains on the Ca-ATPase (Bishop et al., 1988) and thus we can clarify the relative roles of the reactive moiety versus the spectroscopic reporter group in determining the probe's specificity.

Modification with Maleimide-Directed Probes. We have characterized the modification by three maleimide-directed probes, i.e., ANSmal, DABmal, and Fmal, with respect to their functional effects on the Ca-ATPase by determining, as a function of the extent of probe modification, both overall enzymatic activity (by measuring A23187-stimulated Ca-dependent ATP hydrolysis) and formation of phosphorylated enzyme intermediate from ATP (Figure 2). The results indicate that all three probes have the same effects on the functional properties of the Ca-ATPase and that these effects depend only upon the extent of probe modification. It should be noted that the kinetics of labeling of these probes are somewhat different; Fmal modification occurs more slowly than that by either DABmal or ANSmal at very high labeling stoichiometries; however, at the low stoichiometries used in this study, labeling with all probes was equally rapid. Both phosphoenzyme formation and overall ATPase activity are retained with levels of modification up to 4–5 nmol of maleimide bound/mg of SR protein, a level equivalent to about 1 mol of maleimide/mol of ATPase on the basis of the stoichiometry of phosphoenzyme obtained for unmodified SR preparations (Inesi, 1985). At higher probe stoichiometries, i.e., up to twice the concentration of phosphorylatable enzyme intermediate (8–10 nmol/mg of SR), overall enzymatic turnover is progressively inhibited without affecting ATP-dependent phosphorylation, implying that decomposition of the phosphorylated enzyme intermediate is partially inhibited by modification of these residues. No further inhibition of enzymatic activity was observed by further modification up to 12 nmol of maleimide/mol of ATPase (data not shown), suggesting that additional modified residues do not influence the enzyme's function. The same functional characteristics have been previously observed by using NEM and several other maleimide-directed fluorophores to modify the Ca-ATPase (Miki et al., 1981; Yasuoka-Yabe & Kawakita, 1983). These effects are distinct from those of iodoacetamide-directed probe modification of the Ca-ATPase, which do not alter the enzyme's functional properties (Squier et al., 1987); iodoacetamide-directed probes have been localized to cysteines 670 and 674 (Bishop et al., 1988). In addition, prelabeling the Ca-ATPase with a saturating amount of IAEDANS does not alter the time course of subsequent Fmal incorporation (Figure 3).

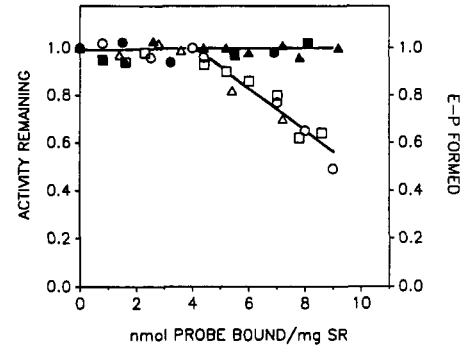

FIGURE 2: Effect of modification by maleimide-directed probes on the A23187-stimulated Ca-dependent ATPase activity (open symbols) and phosphoenzyme formation from ATP (solid symbols). Data is shown from ANSmal (triangles), DABmal (circles), and Fmal (squares). Activities were assayed as described under Experimental Procedures.

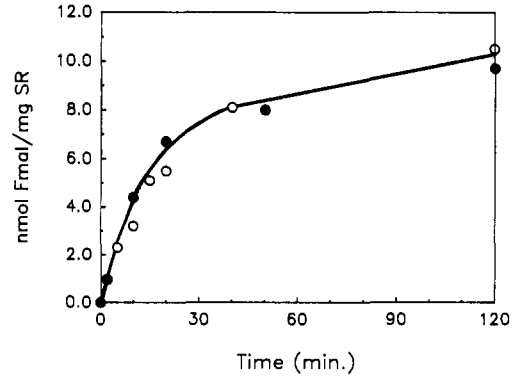

FIGURE 3: Time course of Fmal labeling of SR (○) or SR previously labeled with 9.6 nmol of IAEDANS/mg of SR (●). See Experimental Procedures for procedures for labeling and Fmal quantitation.

Direct visualization of Fmal-labeled protein was obtained on SDS polyacrylamide gels (Figure 4). In agreement with *N*-ethylmaleimide's localization on residues of the A_1 tryptic fragment (Yasuaoka-Yabe & Kawakita, 1983), Fmal fluorescence is associated with the A fragment and, upon further trypsin digestion, with the A_1 fragment. No fluorescence comigrates with either the B or A_2 fragments. Extensive trypsin digestion of Fmal-modified SR followed by centrifu-

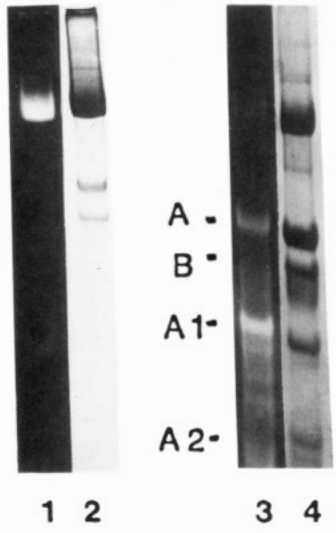

FIGURE 4: Labeling pattern of Fmal–Ca-ATPase on SDS–polyacrylamide gels. Lanes 1 and 2 depict fluorescence (left) and Coomassie Blue staining (right) of Fmal-labeled SR. Lanes 3 and 4 depict fluorescence and Coomassie Blue staining of Fmal–SR digested with trypsin (1:200) for 20 min. A, B, A_1, and A_2 indicate tryptic fragments of the Ca-ATPase.

gation demonstrated that >96% of the fluorescence and 65% of the protein was associated with the soluble peptides rather than with the insoluble membrane pellet. Thus, these labeled residues are located in the extramembranous portion of the A_1 fragment. In similar digestions of other probe-modified SR preparations, i.e., FITC, DABmal, and IAEDANS, >90% of the fluorescence in all cases was associated with soluble peptides confirming the predicted cytoplasmic location of these sites (MacLennan et al., 1985).

Solvent Accessibility of Maleimide-Directed Probes. We investigated the locations of bound maleimide probes on the Ca-ATPase by measuring their accessibility to water-soluble quenchers of fluorescence at varying ANSmal stoichiometries in order to ask whether the change in functional properties observed at higher probe stoichiometries might be a result of involvement of a new and functionally sensitive site or, alternatively, if extensive modification results in alterations of the native protein structure. Quenching studies have been shown to be a sensitive measure of the extent to which groups are buried within the protein structure and thus of site heterogeneity (Eftink & Ghiron, 1981). Addition of the quencher iodide to suspensions of ANSmal-labeled SR decreased both the steady-state fluorescence intensity and the excited-state lifetimes to the same degree (Figure 5), indicating that quenching occurs via collisional encounters between fluorophore and quencher; thus the resulting slopes are directly related to the rate of diffusional encounter between fluorophore and quencher (Eftink & Ghiron, 1976). The observed linearity of the Stern–Volmer plots and similar solvent accessibility at differing labeling stoichiometries indicates, over the tested range of labeling stoichiometries, similar environments for the probes; the presence of multiple populations would result in downward curvature of the plot. These results further suggest that the observed inhibition of enzymatic function at higher labeling stoichiometries (see Figure 2) is not a result of a large distortion of the protein structure near the maleimide sites..

Comparison of the slopes (K_{SV}) of the Stern–Volmer plots from ANSmal free in solution and from ANSmal bound to the Ca-ATPase demonstrates that bound ANSmals are not completely available to the solvent and thus are somewhat shielded by the protein. Both the solvent accessibilities and specificity of maleimide-directed probes to a single population

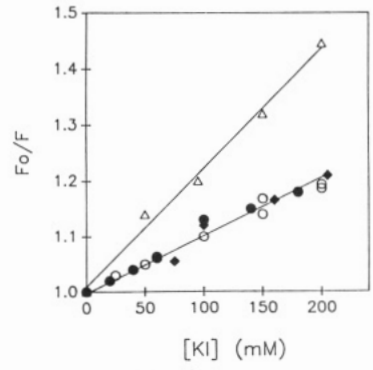

FIGURE 5: Collisional quenching of ANSmal–cysteine free in solution (△) and ANSmal-Ca-ATPase (○, ●, ◆) by iodide. Quenching of ANSmal bound to the Ca-ATPase was measured by steady-state fluorescence intensities at labeling stoichiometries of 4.2 (○) and 8.6 (●) nmol/mg SR, and by excited-state lifetimes (⟨τ⟩, ◆) at 8.6 nmol/mg of SR at 0.04 mg of protein/mL and 23 °C in 20 mM MOPS buffer (pH 7.0), 80 mM KCl, 5 mM $MgCl_2$, and 0.5 mM EGTA. Excitation was at 307 nm; emission was measured at 460 nm for steady-state measurements and through a Corning 3-74 cutoff filter for lifetime decays.

Table I: Solvent Accessibility of Extrinsic and Intrinsic Probes on the Ca-ATPase[a]

probe	K_{SV} (M^{-1})	τ (ns)	k_q ($\times 10^{-9}$ M^{-1} s^{-1})	k_q^p/k_q^s
ANSmal–SR[b]	0.93 (±0.03)	6.4	0.14	0.40
ANSmal–Cys	2.29 (±0.06)	6.4	0.36	
Fmal–SR[c]	3.20 (±0.09)	4.0	0.80	0.38
Fmal–Cys	8.11 (±0.15)	3.8	2.13	
IAEDANS–SR[d]	1.47 (±0.06)	16.4	0.09	0.23
IAEDANS–Cys	3.49 (±0.1)	8.9[e]	0.39	
FITC–SR[f]	3.34 (±0.1)	4.0	0.84	0.48
FITC–Lys	6.7 (±0.1)	3.8	1.76	
tryptophan	1.6 (±0.1)	4.6	0.35	0.06
NATA[g]	17.3[h]	2.95	5.86	

[a] k_q^p and k_q^s were obtained from the slopes of Stern–Volmer plots (K_{SV}) and lifetimes (τ_0) of probes either bound to the Ca-ATPase or free in solution, respectively, where $F_0/F = 1.0 + K_{SV}[Q]$ and $K_q = K_{SV}\,\tau_0^{-1}$. Acrylamide was used to quench the fluorescence of ANSmal, IAEDANS, and tryptophan; iodide was used to quench Fmal and FITC. Experimental conditions were as described in the legend to Figure 5. Errors represent SEM from 2–3 measurements. [b] Probe stoichiometries of samples were 4.2 and 8.4 nmol of ANSmal/mg of SR. [c] Probe stoichiometry of sample was 9.6 nmol of Fmal/mg of SR. [d] Probe stoichiometry of sample was 9.0 nmol of IAEDANS/mg of SR. [e] Taken from Hudson and Weber (1976). [f] Probe stoichiometry of sample was 5.3 nmol of FITC/mg of SR. [g] *N*-acetyl-L-tryptophanamide (NATA). [h] Taken from Eftink and Ghiron (1977).

of residues over this labeling stoichiometry can be better appreciated if their accessibilities are compared to those of other probes specifically bound to known residues of the Ca-ATPase. Therefore, we compared the ratios of the bimolecular quenching constants ($k_q = K_{SV}\,\tau^{-1}$) obtained from each probe covalently bound to the protein to that of the same probe free in solution. This approach yields a quantitative measure of the extent of protection that the protein provides from soluble quencher to the probe, since differences in both the lifetime and quenching efficiency are taken into account (Lakowicz, 1983). A comparison of these ratios from several extrinsic and intrinsic probes of the Ca-ATPase, using either iodide or acrylamide as quenching reagents, is shown in Table I. The solvent accessibilities obtained for both ANSmal and Fmal reflect a degree of exposure on the protein structure that is intermediate between that of the more exposed FITC and the less exposed IAEDANS. We emphasize that the sensitivity of the quenching technique to any label heterogeneity, and the similar solvent accessibility obtained for ANSmal and Fmal,

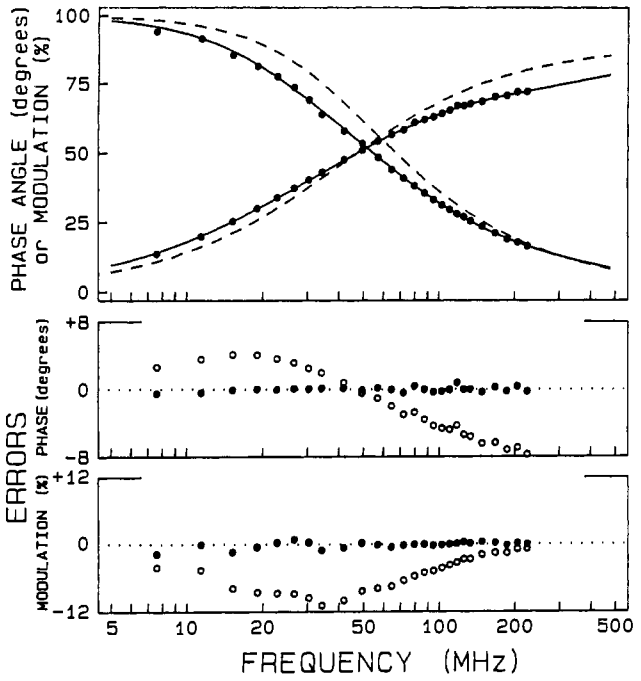

FIGURE 6: Frequency response of ANSmal emission from the Ca-ATPase. The circles show the data and the curves the best single- (dashed line) and triple- (solid line) exponential fits to the data. The lower panels show the deviations between the data and the best single- (○) and triple- (●) exponential fits.

independent of the labeling stoichiometry (i.e., up to 9.6 nmol/mg of SR), indicate that these maleimide derivatives label a protein environment distinct from that of FITC and IAEDANS and consistent with earlier labeling kinetics and sequencing results obtained by using NEM (Saito-Nakatsuka et al., 1987; Yamashita & Kawakita, 1987). In contrast to these probes of the cytoplasmic domains, the intrinsic tryptophans are substantially more protected from the aqueous medium, consistent with their predicted location within transmembrane segments (MacLennan et al., 1985).

Lifetime of ANSmal. Measurements of lifetimes for these fluorescent probes bound to the protein allow the characterization of both the probe's local environment and its location with respect to other bound probes, since fluorophores are sensitive to the polarity of their environment and can serve as energy transfer donors in the proximity of an appropriate acceptor, which acts to decrease the donor's lifetime. Therefore, the lifetime of ANSmal was measured from the frequency response (see Experimental Procedures for details) of the emission of bound ANSmal (Figure 6); as the frequency of the incident light is increased, the emitted light is demodulated and its phase angle increases relative to the incident light. This data requires a three-exponential model to adequately describe the data as demonstrated by the decrease in x_R^2 from 92 to 1.66 to 0.82 for one-, two-, and three-exponential fits, respectively (Table II). For this data (50 degrees of freedom) the 2-fold decrease in x_R^2 indicates that, with greater than 99% confidence, the three- (rather than the two-) exponential model is required (Bevington, 1969). Fitting to a four-exponential model does not significantly improve the fit, giving a x_R^2 of 0.78.

It has sometimes been assumed that the physical basis of such a heterogeneous fluorescence decay is the existence of multiple probe sites on the protein with each decay time representing one site (Birmachu et al., 1989). However, this data can be fit equally well by a model in which the intensity decay is fit to a Gaussian distribution of decay times (Figure 7; Alcala et al., 1987; James et al., 1987; Lakowicz et al., 1987). With the same number of floating parameters, the x_R^2 values for a bimodal distribution are essentially equivalent to those found with the model of three discrete decay times (Table II), indicating that there need be no unique relationship between the number of residues labeled and the exponential components required to fit the data. Therefore, although the heterogeneous intensity decay reflects the fluorophore's environment on the protein (Beechem & Brand, 1985), the number of probe sites cannot be extracted solely from the number of components obtained from data analysis, since this depends upon the assumed model (e.g., a multiexponential model of the intensity decay). While the multiexponential and lifetime distribution models provide an equivalent description of the data, we have chosen, for further analysis, to utilize the more commonly used multiexponential model to describe the intensity decay.

In order to further resolve any possible heterogeneity in labeling, especially at the higher labeling stoichiometries, we have measured the lifetime of ANSmal at various labeling stoichiometries. It should be noted that protein sequencing methods generally fail to recover the entire fraction of the initial bound label and therefore may miss significant minor sites, whereas fluorescence measurements directly monitor the fluorophore's environment in the protein's native conformation and are therefore sensitive to site heterogeneity. We find that neither the decay times (τ_i) of ANSmal nor their relative amplitudes (α_i) vary with increasing stoichiometries of labeling (Figure 8), emphasizing that there are not significant alterations in the environment whether reported by one or two probes bound per ATPase molecule, providing another indication that a homogeneous protein environment is derivatized

Table II: Multiexponential Analysis of ANSmal Emission from the Ca-ATPase[a]

x_R^2	τ_i(ns)	α_i
92.3	5.42	1.00
1.66	1.53	0.335
	6.80	0.665
0.82	0.51	0.205
	3.09	0.303
	7.40	0.497

[a] Samples consisted of 0.2 mg of ANSmal-labeled SR/mL of 20 mM MOPS buffer (pH 6.8), 80 mM KCl, 5 mM $MgCl_2$, 0.5 mM EGTA, 0.6 mM $CaCl_2$, and 0.3 mM myristoyllysophosphatidylcholine at 25 °C; excitation at 307 nm; emission measured through a Corning 3-74 cutoff filter.

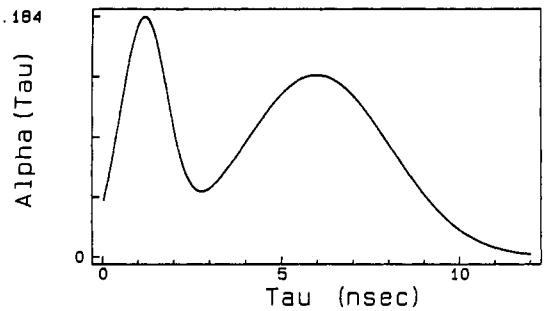

FIGURE 7: Bimodal decay time distribution analysis of ANSmal emission from the Ca-ATPase is described by the table below, where

τ_i (ns)	Γ_i (ns)	g_i	x_R^2
1.15	1.56	0.287	
5.98	4.86	0.713	0.85 (3.61)

τ_i is the mean lifetime, Γ_i is the shape factor, and g_i is the amplitude of the ith component in the distribution. The x_R^2 value for a fit assuming a unimodal decay time is 3.61.

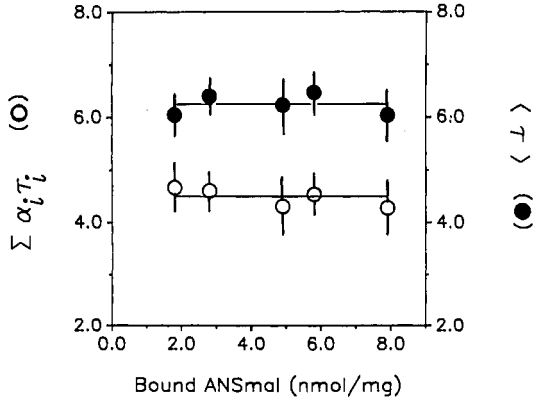

FIGURE 8: ANSmal lifetime as a function of total bound ANSmal. Fluorescence decay parameters, $\sum \alpha_i \tau_i$ (O) or $\langle \tau \rangle$ (●), were calculated (see Experimental Procedures) from the best triple-exponential fits to the data.

Table III: Multiexponential Analysis for Energy Transfer between ANSmal and DABmal

sample	x_R^2	τ_i (ns)	$\sum \alpha_i \tau_i$[a] (ns)	E	r (Å)
ANSmal-SR[b]	0.82	0.51			
		3.09			
		7.40	4.67		
ANSmal	1.18	0.07			
DABmal-SR[c]		2.29			
		6.60	1.45	0.690[d]	36.5

[a] Excitation at 307 nm; emission through Corning 3-74 cutoff filter. [b] Probe stoichiometry of sample was 2.7 nmol of ANSmal/mg of SR in 20 mM MOPS buffer (pH 7.0), 80 mM KCl, 5 mM $MgCl_2$, 0.5 mM EGTA, 0.6 mM $CaCl_2$, and 0.3 mM myristoyllysophosphatidylcholine. [c] Probe stoichiometry of sample was 2.7 nmol of ANSmal and 5.7 nmol of DABmal/mg of SR; same buffer. [d] Efficiency of energy transfer (E) obtained from steady-state fluorescence was 0.645; R_0 = 40.4 Å.

over this range of labeling stoichiometries. These results further rule out both steric interactions between probes and any probe-induced alterations in the protein's conformation near each probe. On the other hand, we observed that the steady-state polarization of ANSmal decreases at higher probe stoichiometries, from 0.310 (±0.008) to 0.256 (±0.005) at 1 mol (4.2 nmol/mg) or 2 mol (8.4 nmol/mg) of bound ANSmal/mol of ATPase, respectively. A likely mechanism for this depolarization is the occurrence of nonradiative energy transfer between two molecules of ANSmal on the same Ca-ATPase polypeptide chain at higher probe stoichiometries; ANSmal's emission and absorption spectrum overlap and thus the same probe can act as both an energy transfer donor and acceptor if these are in proximity.

Resonance Energy Transfer between Maleimide-Directed Probes. Thus, while depolarization of the ANS emission suggests a proximity relationship between these maleimide probes, these data alone are not sufficient to obtain quantitative information regarding the separation between probes (Weber & Daniel, 1966; Dale & Eisinger, 1974); therefore, direct measurements of energy transfer between ANSmal (donor) and DABmal (acceptor) were made. The nonfluorescent acceptor DABmal was utilized in order to optimize the signal due to the donor's measured emission, since the necessity of filtering out sensitized emission of a fluorescent acceptor is eliminated. Frequency domain fluorometry was used to measure the donor's lifetime; the presence of bound DABmal decreases the decay times of ANSmal, increases the amplitudes of the shorter decay times, and decreases its steady-state intensity (Table III), all indicative of resonance energy transfer between these probes. A limitation of using a nonfluorescent

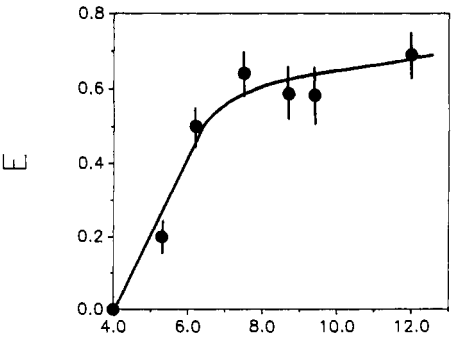

FIGURE 9: Energy transfer from ANSmal to DABmal as a function of total bound maleimide. E (efficiency of energy transfer) was determined from steady-state intensities (λ_{ex} = 340 nm; λ_{em} = 460 nm) of samples having 4.1 nmol of ANSmal bound/mg of SR with varying amounts of bound DABmal up to a total of 12.2 nmol of total maleimide probe/mg of SR in 20 mM MOPS buffer (pH 6.8), 80 mM KCl, 5 mM $MgCl_2$, 0.6 mM $CaCl_2$, 0..5 mM EGTA, and 0.3 mM lysolecithin at 25 °C with 0.05 mg of SR/mL.

acceptor is that the presence of sensitized emission cannot be measured as further evidence of radiationless energy transfer. However, sensitized emission was observed when the fluorescent acceptor, Fmal, was substituted for DABmal, and the calculated distances were the same for both donor–acceptor pairs, consistent with identical sites for both maleimide probes. Finally, the previous result, i.e., that occupancy of both maleimide sites does not affect the lifetime of ANSmal (Figure 8), suggests that the observed changes in donor lifetime in the presence of a maleimide acceptor are not due to changes in the donor's environment. Furthermore, as the stoichiometry of bound acceptor increases, energy transfer increases linearly but does not increase appreciably at probe stoichiometries above 8 nmol/mg (Figure 9), demonstrating that although maleimides can bind in excess of this stoichiometry, energy transfer reflects only the most reactive sites.

The distance between maleimides was estimated from the frequency domain data by using both (1) the discrete multiexponential model, thus assuming a single donor–acceptor distance, and (2) an algorithm that assumes a Gaussian distribution of distances (see Experimental Procedures). The latter analysis has been suggested to be a more appropriate model for probes bound to a flexible polypeptide chain (Gryczynski et al., 1988), as would be expected in the case of the Ca-ATPase. The distribution reflects the degree of static or dynamic disorder resulting from either multiple conformations or structural fluctuations of the polypeptide chain or attached probe (Lakowicz et al., 1987b).

Independent of the assumed model (i.e., a rigid molecule, assumed by the multiexponential model, versus the dynamic structure, assumed by the distance distribution model), the calculated mean separation between ANSmal and DABmal is 36 Å (Tables III and V). However, given that biomolecules are dynamic structures and a considerable body of evidence has arisen to indicate a functional role for their conformational heterogeneity [reviewed by Bennett and Huber (1984)], we feel that the distribution model is likely to be more realistic and therefore have focused on its application here. The recovered distribution between these maleimide-directed probes is characterized by a half-width (hw) of 14 Å (Figure 10a, Table V). Holding the half-width constant at 0.1 Å results in a substantial increase in the x_R^2 value, indicating that the data more strongly support the distribution analysis. Assuming a more complex model involving two mean distances (r_{av}), i.e.,

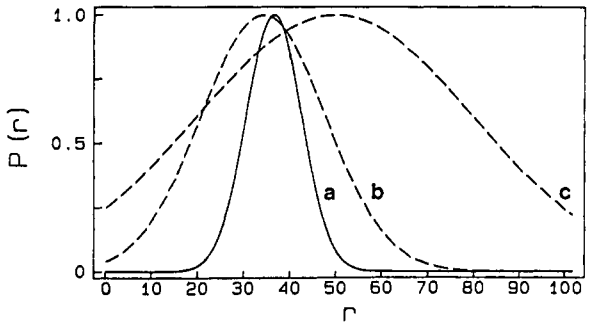

FIGURE 10: Unimodal distance distribution from ANSmal to DABmal (a), IAF (b), and FITC (c).

a bimodal Gaussian distribution, there is no improvement in the fit to the data. Furthermore, the two mean distances and two half-widths recovered from the bimodal Gaussian distribution are identical with each other and with those obtained from the unimodal model, consistent with sequencing results, quenching measurements, and independence of lifetime to probe stoichiometry, all of which indicate two sites with equal affinity for these maleimides and a single donor–acceptor distance.

It should be noted that, in using a distribution analysis, we tested the accuracy of the independently determined parameters in the analysis, e.g., the R_0, the fraction of bound donor with acceptor, and the fraction of donor bound at each site (in bimodal analysis), by treating each as a variable in the analysis. The recovered distribution was not significantly different nor were these parameters significantly altered in order to achieve an optimal fit under these conditions, emphasizing the independence of the recovered distributions from errors that might arise in the determination of spectral properties or quantitation of bound fluorophores.

This approach has been especially informative in the case of the ANSmal–DABmal pair; when the fraction of donors with acceptors (f) is allowed to float, its recovered value is 0.97 (±0.01), as would be expected if these sites were labeled as suggested previously (Yamashita & Kawakita, 1987) so that each site is labeled randomly but, once modified, inhibits the labeling of the second site on the same ATPase molecule. In the bimodal analyses, when the fraction of donor at each site was allowed to float, its recovered value was 0.50 (±0.01) for all donor–acceptor pairs tested, indicating the random labeling of these sites.

Energy Transfer from Maleimide Probes to Other Covalently Bound Probes. In order to characterize the location of the maleimide sites with respect to other defined points within the tertiary structure of the Ca-ATPase, we measured energy transfer between bound maleimides and other covalently bound acceptors, i.e., both FITC, modifying Lys 515 near the nucleotide site, and iodoacetamide probes, modifying the proximal Cys 670 and 674. Energy transfer is exhibited by both donor–acceptor pairs by decreases in the donor's quantum yield (Table IV) and sensitized fluorescein emission (data not shown). Again, by using models in which the distance of separation is described by a unique distance (multiexponential analysis) or the flexibility of biological macromolecules is considered (distance distribution model), the calculated distances between these donor–acceptor pairs are in good agreement: 34–35 Å between ANSmals and the IAF site and 48–49 Å between ANSmals and the FITC. Likewise, the calculated quantum yields obtained from the lifetime data are in good agreement with steady-state measurements of the quantum yield, ruling out any statically quenched population of probes. In contrast is the data from the IAEDANS–DABmal pair, for which the apparent distance derived from the discrete exponential model is considerably different than that derived from either the steady-state data or the ANSmal–IAF pair. However, a distribution analysis of lifetime data from the former pair, which takes into account both distance heterogeneity and fraction of labeled sites, yields good agreement between lifetime and steady-state data. It should be emphasized that since these models assume a single donor–acceptor distance, the values obtained represent apparent distances that most likely result from the average of the transfer rates between two spatially separated maleimides and their acceptor. The heterogeneity in these distances results in distributions that are characterized by substantially larger half-widths than in the case of the single donor–acceptor distance of ANSmal and DABmal (distribution a, Figure 10; Table V). In addition, the distribution for the ANSmal–FITC pair is considerably broader than that for the ANSmal–IAF pair, reflecting a greater heterogeneity of distances contributing

Table IV: Multiexponential Analysis of Energy Transfer between Maleimide and Other Probes of the Ca-ATPase[a]

sample	τ_i (ns)	α_i	$\sum\alpha_i\tau_i$ (ns)	x_R^2	E	R_0 (Å)	r (Å)
ANSmal–SR[b]	0.10	0.278					
	2.78	0.271					
	7.37	0.451	4.11	0.86			
ANSmal-FITC-SR[c]	0.11	0.375					
	2.71	0.240					
	7.25	0.298	2.85	0.95	0.318[d]	42.1	48.2
ANSmal–IAF–SR[e]	0.05	0.685					
	2.46	0.147					
	6.87	0.167	1.54	1.04	0.625[f]	41.5	34.6
IAEDANS–SR[g]	1.61	0.388					
	18.16	0.612	11.73	1.3			
IAEDANS-DABmal-SR[h]	1.88	0.590					
	16.79	0.410	7.99	1.6	0.318[i]	40.5	46.3

[a] Experimental conditions were as described in Table II. [b] Probe stoichiometry of sample was 4.2 nmol of ANSmal/mg of SR; excitation was at 307 nm; emission was measured through Corning 3-74 cutoff and 7-59 band-pass filters. [c] Probe stoichiometry of sample was 4.2 nmol of ANSmal and 4.8 nmol of FITC/mg of SR; excitation and emission as above. [e] Probe stoichiometry of sample was 4.2 nmol of ANSmal and 8.0 nmol of IAF/mg of SR; excitation and emission as above. [g] Probe stoichiometry of sample was 4.0 nmol of IAEDANS/mg of SR; excitation was at 350 nm; emission was measured through a Schott GG400 cutoff filter. [h] Probe stoichiometry of sample was 4.0 nmol of IAEDANS and 4.1 nmol of DABmal/mg of SR; excitation and emission as above. [i] E determined from steady-state fluorescence intensity was 0.75 (±0.02).

Table V: Distance Distribution Analysis of Resonance Energy Transfer between Spectroscopic Probes on the Ca-ATPase[a]

donor/acceptor		r_{av} (Å)	hw_i (Å)	x_R^2
ANSmal/DABmal	unimodal	36.0 (±0.5)	13.9 (±1)	1.22
			⟨0.1⟩	15.7
	bimodal	36.2 (±1.1)	13.8 (±2.4)	
		35.9 (±1.2)	13.9 (±2.4)	1.29
ANSmal/IAF	unimodal	33.7 (±4)	31.1 (±2)	1.7
			⟨0.1⟩	40.3
	bimodal	31.9 (±1.6)	20.2 (±3.2)	
		46.8 (±0.9)	19.0 (±2.8)	1.0
IAEDANS/DABmal	unimodal	33.3 (±3.2)	13.2 (±5)	3.8
			⟨0.1⟩	22.3
	bimodal	28.4 (±0.9)	10.2 (±4)	
		37.2 (±1.2)	6.6 (±5)	1.8
ANSmal/FITC	unimodal	49.0 (±6)	69 (±10)	1.4
			⟨0.1⟩	14.9
	bimodal	41.6 (±1.6)	9.5 (±2.5)	
		77.2 (±7.5)	6.5 (±2.2)	1.1

[a] Experimental conditions were as described in Table IV. Errors represent one standard deviation around the recovered value. ⟨⟩ indicates that the value was held constant in the fitting.

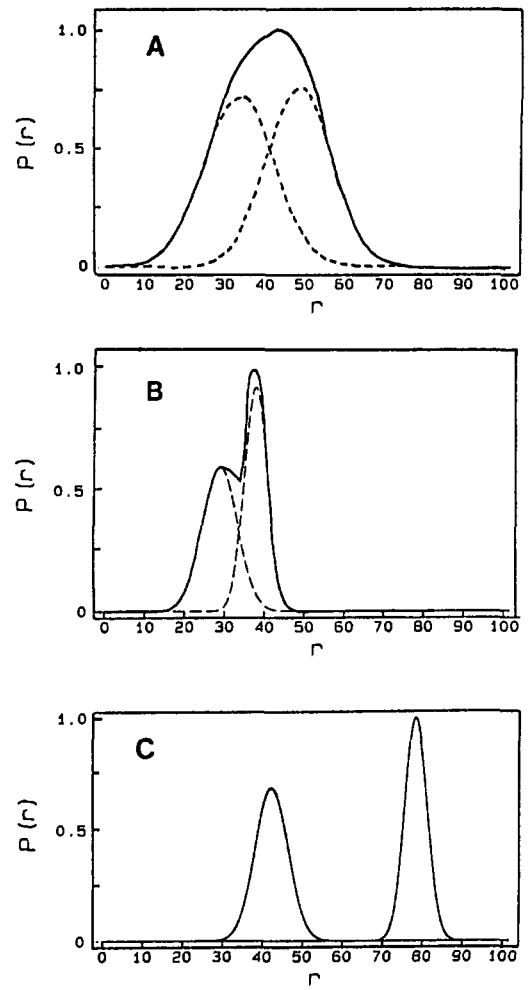

FIGURE 11: Bimodal distance distributions between ANSmal and IAF (A), IAEDANS and DABmal (B), and ANSmal and FITC (C). Dashed lines in (A) and (B) show the overlapping components (having r_{av} and hw as designated in Table V) that contribute to the bimodal distribution.

to the mean distance of the former.

Assumption of a bimodal model to analyze the data from the donor–acceptor pair ANSmal and IAF results in decreased x_R^2 values relative to the unimodal model, indicating with >98% confidence that a bimodal model is necessary to describe the data. In addition, the recovered half-widths are decreased relative to those from the unimodal model (Table V) and are consistent with values in which unique donor–acceptor distances have been measured (Gryczynski et al., 1988). Both the similarity in values of the two recovered mean distances and the width of each component of the distribution (Figure 11A) result in substantial overlap so that the sum of these components, i.e., the bimodal distribution, resembles a somewhat asymmetric unimodal distribution.

To further test the appropriateness of this bimodal assumption, we measured energy transfer between these sites using different chromophores, i.e., the iodoacetamide derivative IAEDANS as the donor and the maleimide DABmal as the acceptor (Figure 11, Tables IV and V). The fit of this data to a bimodal distribution shows a significant improvement in comparison to that for a unimodal model, i.e., a two-fold reduction in x_R^2 indicates that, given the 24 degrees of freedom, there is a greater than 99% likelihood that the bimodal distribution is necessary to describe the data. Like the data from the ANSmal–IAF pair, the two recovered mean distances have similar values, but the half-widths are significantly narrower; thus the resulting summed distribution exhibits a more clearly

Table VI: Multiexponential Analysis of Energy Transfer between Intrinsic Tryptophans and Maleimide Probes on the Ca-ATPase[a]

sample	x_R^2	τ_i (ns)	α_i	$\sum\alpha_i\tau_i$ (ns)	E	r_{app} (Å)
SR[b]	29.3	3.91	1.00			
	2.6	1.85	0.511			
		5.57	0.489	3.67		
DABmal-SR[b]	23.0	3.85	1.00			
	1.4	1.35	0.462			
		3.85	0.538	3.31	0.098[c]	35.1
SR[d]	10.6	4.48	1.00			
	1.4	0.91	0.333			
		5.03	0.667	3.66		
ANSmal-SR[d]	22.6	4.22	1.00			
	2.6	0.73	0.343			
		4.93	0.657	3.48	0.049[e]	42.3

[a] Experiments were performed with 0.1 mg (labeled or unlabeled) of SR/mL in a buffer of 20 mM MOPS (pH 6.8), 80 mM KCl, 5 mM $MgCl_2$, 0.5 mM EGTA, 0.6 mM $CaCl_2$, and 0.3 mM myristoyllysophosphatidylcholine at 25 °C. [b] Excitation at 298 nm; emission through Schott 320 and Corning 7-51 cutoff filter. [c] Energy transfer efficiency (E) measured from steady-state fluorescence = 0.091 (R_0 = 28.0 Å). [d] Excitation at 298 nm; emission through a 340 interference filter. [e] Energy transfer efficiency (E) measured from steady-state fluorescence = 0.058; R_0 = 29.4 Å.

bimodal shape (Figure 11B). While the data from both donor–acceptor pairs are qualitatively similar, there are some quantitative differences in the recovered mean distances and half-widths that may arise from differences in chemical, spectral, or dynamic properties in the chromophores used. However, the distribution from the IAEDANS–DABmal pair lies well within the range of the broader distribution from the ANSmal–IAF pair, indicating that these complementary measurements provide an accurate measure of the distances between these covalently bound probes. Likewise, two distinct and nonoverlapping components are recovered when the data obtained from the ANSmal–FITC pair is fit to a bimodal model (Figure 11). The half-widths are dramatically decreased relative to those of the unimodal distribution. In this case, there is a more modest decrease in x_R^2 values when the bimodal model is compared to the unimodal model; however, the improvement in x_R^2 values indicates with greater than 84% confidence that the bimodal model is necessary to describe the data. It should be noted that one of the recovered mean distances (77 Å) is near the limits of detection for this donor–acceptor pair and this is reflected by the larger confidence intervals for this distance (Table V). We want to emphasize that a bimodal model best describes the data obtained from energy transfer between maleimides and other covalently bound probes, as evidenced by decreases in both x_R^2 values and recovered half-widths relative to the unimodal model. In addition the mean distances recovered from the bimodal model differ from those recovered from the unimodal model. These characteristics contrast with those from similar analyses of the single donor–acceptor distance between maleimide probes.

As a means of localizing the maleimide sites with respect to the bilayer, energy transfer was measured from the intrinsic tryptophans, since 12 out of the 13 total tryptophans are predicted to be located within transmembrane helices at positions near both cytoplasmic and lumenal surfaces of the bilayer. Energy transfer was measured from both the lifetime and the steady-state intensity of these tryptophans with either ANSmal or DABmal as acceptors. A two-exponential model adequately describes the fluorescence decay of these tryptophans (Table VI), whether in the presence or absence of either maleimide acceptor; the extent of energy transfer calculated from decreases in intensity decays was small for both acceptors, 0.049 and 0.098 for ANSmal and DABmal, respectively. Changes in the steady-state quantum yield agree with the

lifetime-resolved measurements, indicating that the transfer efficiency is not the result of the complete quenching of only a few tryptophans. In addition, sensitized emission of ANSmal was observed. The apparent distances between 13 tryptophans and two ANSmals or two DABmals calculated from the decay parameters correspond to 47 and 41 Å, respectively. However, these values are likely to represent overestimates, since we expect that about six of the 13 tryptophans are located at the lumenal surface of the 40-Å bilayer and therefore do not transfer energy to acceptors. Thus, the apparent distance from the tryptophans capable of transferring enegy to maleimide acceptors may be 5–6 Å less. Due to both the complexity of data interpretation and the small transfer efficiency observed, in this case, we did not fit these decays to a more specific (e.g., multimodal) model.

Discussion

We have localized covalently bound maleimide-directed chromophores within the tertiary structure of the Ca-ATPase; these probes modify amino acid residues within the region that includes the phosphorylation site and are important to the rate-limiting turnover of the phosphorylated enzyme, therefore providing a means to directly measure the structure within this essential region. Maleimide derivatives have been used extensively to monitor functionally relevant conformational changes of the Ca-ATPase (Thomas & Hidalgo, 1978; Miki et al., 1981; Yasuoka-Yabe & Kawakita, 1983; Yamamoto et al., 1984; Bigelow & Thomas, 1987), and their characterization is important to meaningful interpretation of these findings. Moreover, the placement of these covalent maleimide sites within the tertiary structure in relation to other site-specific fluorescent probes, i.e., iodoacetamide-directed chromophores (Cys 670 and 674) and FITC (Lys 515), now permits us to more realistically localize these probes with respect to the tertiary structure of the native protein and provides a means of further testing protein-folding predictions (Brandl et al., 1986).

Site Characterization. Functional effects resulting from maleimide modification of the Ca-ATPase (Figure 2) suggest that all three derivatives modify the same sites and that these labeling characteristics are analogous to those of NEM (modifying Cys 344 and 364), but distinct from those of iodoacetamides that modify cysteines 670 and 674 (Figure 3). Likewise, quenching studies (Table I) demonstrate that ANSmal and Fmal bound to the Ca-ATPase have the same solvent accessibilities and that this environment is distinct from those of other covalently bound cytoplasmic probes. Consistent with their rapid labeling kinetics (Figure 3), maleimides at these sites are relatively accessible to the surrounding aqueous solvent, especially in contrast to the dramatically decreased accessibility of the intrinsic tryptophans predicted to lie within the bilayer. Previous sequencing of NEM-modified peptides indicated that the two most reactive sites are derivatized randomly; in agreement, we find that both lifetimes and solvent accessibilities of fluorescent maleimides indicate the same microscopic environments whether at high or low probe stoichiometries. The abrupt change in slope of the titration of energy transfer between donor and acceptor maleimides (Figure 8) identifies these most reactive sites as those involved in energy transfer.

It has been suggested that the functional inhibition observed at high probe stoichiometries may be due to distortion of the native conformation of the Ca-ATPase by two bulky groups attached to the polypeptide chain near the phosphorylation site (Kawakita & Yamashita, 1987); however, we find no evidence for any significant change in solvent accessibility for these probes when two maleimides are bound per ATPase. This is an important consideration when comparing structural dimensions obtained from the Ca-ATPase modified at low labeling stoichiometries (between maleimides and other covalent probes) with those obtained at high labeling stoichiometries (between maleimides).

Localization of Maleimides by Resonance Energy Transfer. Fluorescence measurements provide a means to probe the native folded and functionally competent conformation of the enzyme in solution. We use frequency domain fluorescence spectroscopy, whose dynamic range permits us to recover the entire intensity decay characteristic of these fluorophores and provides a sensitive measure of the heterogeneity in the fluorescence decays that are a result of a range of donor–acceptor distances (Lakowicz et al., 1987b). In the case of the distance separating the two maleimides, the recovered distribution of distances is relatively narrow (Figure 10), with a half-width (14 Å) comparable to that observed from both proteins and synthetic molecules having single donors and single acceptors (Gryczynski et al., 1988), and is therefore consistent with a single distance between probes attached to a flexible molecule. The large spatial separation between maleimide-directed probes, i.e., 36 Å, in good agreement with proximity measurements between spin-labeled maleimides bound to the Ca-ATPase (Horvath et al., 1990), indicates that one cannot treat chromophores directed at these residues as a single locus. This creates a potential complication in the interpretation of energy transfer measurements between these and other site-directed probes. In this regard, measurements of the mean transfer efficiency (obtained from either steady-state data or multiexponential analysis of lifetime data) do not provide a realistic approximation of these donor–acceptor separations. A more realistic description of these data was obtained by utilizing the resolution inherent in the frequency-domain measurement to recover multiple distances, where bimodal distributions (Figure 11) model both the two donor–acceptor distances and the conformational flexibility that biological macromolecules are known to exhibit (Bennett & Huber, 1984).

For example, there is considerable heterogeneity in the apparent single distance estimated between maleimides and FITC (as reflected in the large half-width; Figure 10, Table V) that can be resolved with a bimodal distribution of distances into two significantly different mean distances as evidenced by decreased half-widths and χ^2 values. In contrast, with IAF as the acceptor, bimodal analysis resolves two similar distances (Table V), consistent with the smaller extent of distance heterogeneity reflected by the unimodal half-width. Thus, while these unimodal distributions accurately reflect the extent of distance heterogeneity, information concerning individual sites is lost. The ability to recover the two donor–acceptor distances from the donor's frequency response represents a significant advance in the use of fluorescence resonance energy transfer for biological systems, where specific and selective labeling of a single residue is not always possible.

The chromophores used to measure distances between sites on the head of the Ca-ATPase have proven to be ideal probes of these distances, since for each donor–acceptor pair the measured distance was close to the Forster distance (R_0), where the sensitivity to energy transfer is the greatest. However, the extent of energy transfer between intrinsic tryptophans and either of the maleimide probes is considerably less relative to the Forster distance and consequently limits the resolution available from the data. Moreover, the heterogeneity inherent in the fluorescence decay of 13 intrinsic

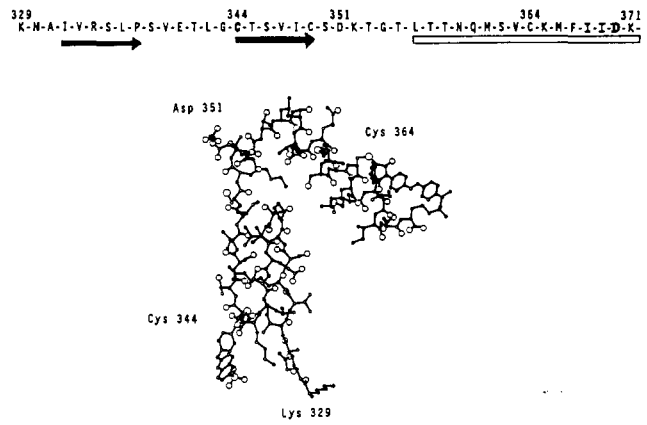

FIGURE 12: Molecular modeling of polypeptide segment in the vicinity of cysteines 344 and 364. Following the arrangement of predicted secondary structural elements suggested previously (MacLennan, 1985), 43 amino acids (Lys 329–Lys 371) are arranged as two parallel β-sheets followed by an α-helix; the second β-sheet and the β-helix bracket a six amino acid sequence containing the enzyme's phosphorylation site (Asp 351), shown here with bound phosphate (phosphorus represented by a filled circle). The sequence predictions are indicated as arrows for the β-sheets and an open bar for the α-helix. In this model ANSmal is depicted bound at the maleimide ring to the cysteinyl (344) sulfur; DABmal is similarly depicted as bound to cysteine 364. The chromophore to chromophore distance is 36.1 Å.

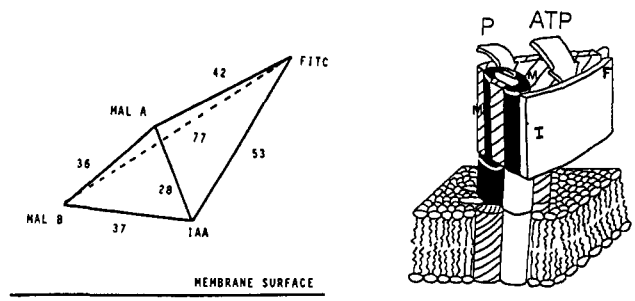

FIGURE 13: Model of spatial relationship of fluorophore sites relative to each other. The left-hand panel depicts sites labeled by FITC, iodoacetamide derivatives (IAA), and maleimide derivatives (MAL A and MAL B). Numbers indicate the mean distances (angstroms) recovered from distance distribution of frequency-domain fluorescence spectroscopy except for the distance between IAA and FITC; this distance was calculated from the frequency-domain fluorescence decay parameter ($\sum \alpha_i \tau_i$) of IAEDANS with FITC as the acceptor. The right-hand panel depicts a placement of these probe sites with respect to the three-dimensional structure of the Ca-ATPase that is consistent with this data and tertiary structural data (Taylor et al., 1984; Castellani et al., 1986; Stokes & Green, 1990). This cartoon model of the Ca-ATPase is based on a previous predicted secondary structure (Brandl et al., 1986) and shows a possible folded structure of the A_1 (hatched), A_2 (solid), and B (white) tryptic fragments. The cylinders depict transmembrane and stalk helices shown in a clustered configuration (however, this is not meant to depict any specific arrangement of these helices); the cytoplasmic head of the Ca-ATPase forms a trigonal arrangement with the A_1 tryptic fragment folded behind the B tryptic fragment forming a cleft for ATP binding. The phosphorylation site at Asp 351 on the A_1 fragment is shown. This model is scaled to be consistent with a membrane thickness of 40 Å, the cytoplasmic head as 40 × 50 × 65 Å and centered 35 Å above the bilayer, and a 28-Å diameter stalk that extends 16 Å from the ATPase head to the bilayer surface. Comparison of the predicted number of residues involved in amphipathic stalk helices with the relatively short stalk region observed (Taylor et al., 1984) suggests that parts of these five helices may interact in some manner with the head region. Possible probe sites are designated by the letters F for FITC, I for iodoacetamide derivatives, and M for maleimide derivatives.

tryptophans in the presence of two spatially separate maleimide probes introduces considerable complexity into the interpretation of this data. Nevertheless, these data (Table VI) suggest a range of distances corresponding to the closest approach of one or more tryptophans.

Structural Model of Maleimide Probes and Surrounding Peptide. In order to appreciate the size of these chromophores with respect to the protein's structure, we modeled a small (<5% of the total protein) portion of the Ca-ATPase and included donor and acceptor maleimides (Figure 12). Choosing a 43-residue polypeptide segment in the region of the NEM-modified residues, we included an attached ANSmal and attached DABmal at cysteines 344 and 364. The depicted structure follows the secondary structure predictions of two β sheets and an α helix; these features are arranged as previously suggested, in analogy to known structures of nucleotide-binding regions of kinases (MacLennan et al., 1985) and so that the distance between chromophores is 36 Å. In addition, the model has been energy-minimized to prevent overlap of amino acid side chains. Interestingly, different orientations of the probes, by rotations of the bond connecting the cysteinyl sulfur to the maleimide ring of the probe, alters the distance between chromophores by approximately 15 Å, similar to the measured half-width (Figure 10, Table V) about the mean distance separating these probes. Therefore, it is plausible that the recovered half-width could be accounted for by differing probe orientations, assuming the absence of any steric constraints imposed on the probe by portions of the protein's structure that are not considered in this model. The modification of these cysteines and the measured distance between chromophores is reasonably consistent with the suggested arrangement of the predicted secondary structural elements in the region of the phosphorylation site.

Model of Spatial Relationships of Probes. The spatial relationship of these probes with respect to one another is illustrated by the model in Figure 13, in which the arrangement of these dimensions results in a shallow pyramid approximately 11 Å high, i.e., from the peak (MAL A) to the plane of the elongated triangle defined by the other maleimide site (MAL B), the iodoacetamide, and the FITC site. The distance between the iodoacetamide and FITC sites was obtained from previous measurements using frequency data at 10 MHz (56 Å; Squier et al., 1987) and a more recent refinement of this measurement using a wide range of frequencies (2–200 MHz) (53 Å; unpublished observations), in good agreement with other FRET measurements from the time domain using these probes (Birmachu et al., 1989). Other dimensions represent the mean distances (r_{av}) obtained from distance distribution analysis of frequency-domain data. Since the data do not allow an unambiguous assignment of each distance around maleimides A and B, an alternative model to that illustrated would be one in which the 28- and 37-Å edges of the pyramid are interchanged. However, no combination of angles between sites with this arrangement of dimensions allows the formation of a contiguous pyramid. Therefore, we conclude that the model illustrated is the best arrangement of these distances.

We can further consider the spatial relationship of these sites in reference to the native protein structure. The extramembranous portion of the Ca-ATPase is predominantly on the cytoplasmic side of the SR membrane; some resolution of this domain has been possible through imaging techniques applied to crystalline arrays of the Ca-ATPase (Taylor et al., 1984; Castellani et al., 1985; Stokes & Green, 1990). These show a pear-shaped lobe (65 × 40 × 50 Å) connected to the bilayer by means of a narrow stalk structure with the entire cytoplasmic protein extending about 65 Å above the bilayer. All residues modified by the probes used in these experiments are found to be associated with extramembranous peptides and

are predicted to be located within regions that are generally assumed to correspond to the pear-shaped lobe observed in tertiary structural studies (Brandl et al., 1986). Estimates of distance to lipid fluorophores have localized bound FITC at a distance >60 Å above the bilayer surface and thus relatively high on the cytoplasmic portion of the Ca-ATPase (Gutierrez-Merino et al., 1987). Our energy transfer measurements demonstrate that there is a relatively large separation between either of the maleimides relative to FITC but a small separation of a least one maleimide site relative to the lanthanide praseodymium, which probably binds to the stalk (Tables IV and V; Squier et al., 1987, 1990). Our measurements between tryptophans and maleimides suggest that at least one of the maleimides is 35–40 Å from the bilayer surface, i.e., at an intermediate position on the cytoplasmic head; similar measurements between tryptophans and IAEDANS suggest that iodoacetamide sites are similarly located with respect to the bilayer surface (36–40 Å away; Gryczynski et al., 1989). Therefore the orientation shown (Figure 13A) is a possible arrangement of these fluorophores relative to the membrane surface, i.e., FITC as the farthest site from the membrane, set relatively high on the cytoplasmic head of the ATPase; both the iodoacetamide site and one of the maleimide sites (MAL B) are placed closer to the membrane surface.

It has been suggested that the two nucleotide-binding domains of the Ca-ATPase fold in a manner similar to that observed for the bilobed crystal structures of nucleotide-binding proteins, e.g., phosphoglycerate kinase and hexokinase (MacLennan et al., 1985), implying that the alternating α-helices and β-sheets of the A_1 tryptic fragment are juxtapositioned (and parallel with the bilayer normal) with those of the B tryptic fragment; the antiparallel β-sheets of the A_2 fragment form a third side of a trigonal structure as illustrated in the cartoon (Figure 13B). Such an arrangement would form a cleft between the A_1 and B domains for nucleotide binding, corresponding to the 40 × 50 × 65 Å cytoplasmic head of the ATPase observed from 3D images. The pyramidal arrangement of maleimide (modifying residues of the A_1 fragment), iodoacetamide (modifying residues of the B fragment), and FITC (also modifying residues of the B fragment) sites can be readily superimposed on a structure of these dimensions; some changes in tilt of the pyramid can be accommodated without altering the limits imposed on its position, i.e., the assignment of each probe in the cytoplasmic portion of a particular tryptic fragment and the high placement of FITC and intermediate position of one maleimide relative to the membrane surface. Thus this model provides a reasonable agreement between a hypothetical three-dimensional model based on a simple folding pattern of the predicted secondary structure (Brandl et al., 1986), dimensions from imaging techniques applied to crystalline arrays of the Ca-ATPase (Taylor et al., 1984; Castellani et al., 1985; Stokes & Green, 1990), and measured distances between site-directed probes covalently bound to the native protein structure in solution (Squier et al., 1987; this study).

Of additional interest with respect to this model is the location of the high-affinity calcium binding sites on the Ca-ATPase. Spectroscopic lanthanides have been used to probe these sites (Highsmith & Head, 1983; Highsmith & Murphy, 1984; Scott, 1985; Herrmann & Shamoo, 1988; Klemens et al., 1988). However, it has remained a controversy as to whether the calcium sites are close to or distant from the nucleotide-binding region; the interpretation of these results is complicated by the observation that at millimolar concentrations lanthanides also bind to magnesium sites on the Ca-ATPase (Highsmith & Head, 1983). In this respect, we have found, using the lanthanide praseodymium as an energy transfer acceptor, that nanomolar concentrations displace high-affinity calcium without interfering with magnesium-dependent phosphoenzyme formation and bind to sites that are relatively close (14–18 Å) to both maleimide and iodoacetamide sites (Squier et al., 1990). The distant location of the latter probes from FITC implies that bound lanthanides are also distant from the nucleotide region, emphasizing the importance of long-range interactions between nucleotide and transport sites for coupled ion transport.

ACKNOWLEDGMENTS

This work was performed in part at the Center for Fluorescence Spectroscopy, University of Maryland at Baltimore, School of Medicine. We thank Mayer Fishman for the construction of the molecular model depicted in Figure 11 using the Quanta program on a Silicon Graphics workstation; we thank Tom Squier for his many insightful discussions regarding this work.

Registry No. ATPase, 9000-83-3; ANSmal, 73376-23-5; DABmal, 87963-80-2; Fmal, 131545-96-5; Cys, 52-90-4; Asp, 56-84-8; FITC, 3326-32-7; IAF, 63368-54-7; IAEDANS, 36930-63-9.

REFERENCES

Alcala, J. R., Gratton, E., & Prendergast, F. G. (1987) *Biophys. J. 51*, 925–936.

Beechem, J. M., & Brand, L. (1985) *Annu. Rev. Biochem. 54*, 43–71.

Bennett, W. S., & Huber, R. (1984) *CRC Crit. Rev. Biochem. 15*, 291–384.

Bevington, P. R. (1969) *Data Reduction and Error Analysis for the Physical Sciences*, McGraw-Hill, New York.

Bigelow, D. J., & Thomas, D. D. (1988) *J. Biol. Chem. 262*, 13449–13456.

Bigelow, D. J., Squier, T. C., & Thomas, D. D. (1986) *Biochemistry 25*, 194–202.

Bigelow, D. J., Squier, T. C., & Inesi, D. J. (1988) *Biophys. J. 53*, 225a.

Birmachu, W., Nisswandt, F. L., & Thomas, D. D. (1989) *Biochemistry 28*, 3940–3947.

Bishop, J. E., Squier, T. C., Bigelow, D. J., & Inesi, G. (1988) *Biochemistry 27*, 5233–5240.

Brandl, C. J., Green, N. M., Korczack, B., & MacLennan, D. H. (1986) *Cell 44*, 597–607.

Castellani, L., Hardwicke, P. M. D., & Vibert, P. (1985) *J. Mol. Biol. 185*, 579–594.

Champeil, P., Bastide, F., Taupin, C., & Gary-Bobo, C. M. (1976) *FEBS Lett. 63*, 270–272.

Chen, R. F. (1974) *Anal. Biochem. 57*, 593–604.

Coan, C. R., & Inesi, G. (1977) *J. Biol. Chem. 252*, 3044–3049.

Coan, C. R., Verjovski-Almeida, S., & Inesi, G. (1979) *J. Biol. Chem. 254*, 2968–2974.

Dale, R. E., & Eisinger, J. (1974) *Biopolymers 13*, 1573–1579.

Dale, R. E., & Eisinger, J. (1975) in *Biochemical Fluorescence Concepts* (Chen, R. F., & Edelhoch, H., Eds.) Chapter 4, pp 115–284, Marcel Dekker, New York.

Dale, R. E., Eisinger, J., & Blumberg, W. E. (1979) *Biophys. J. 26*, 161–194.

Englert, A., & Leclerc, M. (1978) *Proc. Natl. Acad. Sci. U.S.A. 75*, 1050–1051.

Eftink, M. R., & Ghiron, C. A. (1976) *Biochemistry 15*, 672–680.

Eftink, M. R., & Ghiron, C. A. (1977) *Biochemistry 16*, 5546–5551.

Eftink, M. R., & Ghiron, C. A. (1981) *Anal. Biochem. 114*, 199–227.
Eshaghpour, H., Dieterich, A. E., Cantor, C. R., & Crothers, D. M. (1980) *Biochemistry 19*, 1797–1805.
Gratton, E., Lakowicz, J. R., Maliwal, B., Cherek, H., Laczko, G., & Limkeman, M. (1984) *Biophys. J. 46*, 479–486.
Gryczynski, I., Wiczk, W., Johnson, M. L., Cheung, H. C., Wang, C. K., & Lakowicz, J. R. (1988) *Biophys. J. 54*, 577–586.
Gryczynski, I., Wiczk, W. Inesi, G., Squier, T. C., & Lakowicz, J. R. (1989) *Biochemistry 28*, 3490–3498.
Guillain, F., Champeil, P., Lacapere, J.-J., & Gingold, M. P. (1981) *J. Biol. Chem. 256*, 6140–6147.
Gutierrez-Merino, C., Monkonge, F. M., Mata, A. M., East, J. M., Levinson, B. L., Napier, R. M., & Lee, A. G. (1987) *Biochim. Biophys. Acta 897*, 207–216.
Haas, E., Katchalski-Katzir, E., & Steinberg, I. Z. (1978) *Biochemistry 17*, 5064–5070.
Hasselbach, W., & Seraydarian, K. (1966) *Biochem. Z. 345*, 159–172.
Herrmann, T., & Shamoo, A. E. (1988) *Mol. Cell. Biochem. 82*, 55–58.
Hidalgo, C., Thomas, D. D., & Ikemoto, N. (1978) *J. Biol. Chem. 253*, 6879–6887.
Highsmith, S., & Cohen, J. A. (1987) *Biochemistry 26*, 154–160.
Highsmith, S. R., & Head, M. R. (1983) *J. Biol. Chem. 258*, 6858–6862.
Highsmith, S. R., & Murphy, A. J. (1984) *J. Biol. Chem. 259*, 14651–14656.
Horvath, L. I., Dux, L., Hankovsky, H. O., Hideg, K., & Marsh, D. (1990) *Biophys. J. 58*, 231–241.
Hudson, E. N., & Weber, G. (1973) *Biochemistry 12*, 4154–4161.
Inesi, G. (1985) *Annu. Rev. Physiol. 47*, 573–601.
Ishi, Y., & Lehrer, S. S. (1986) *Biophys. J. 50*, 75–80.
James, D. R., Turnbull, J. R., Wagner, B. D., Ware, W. R., & Petersen, N. O. (1987) *Biochemistry 26*, 6272–6277.
Kawakita, M., & Yamashita, T. (1987) *J. Biochem. (Tokyo) 102*, 103–109.
Klemens, M. R., Stewart, J. M., Mahaney, J. E., Kuntzwiler, T. A., Sattler, M. C., & Grisham, C. M. (1988) *Serono Symp. Publ. Raven Press 51*, 107–124.
Lakowicz, J. R. (1983) *Principles of Fluorescence Spectroscopy*, Plenum Publishing Corp., New York.
Lakowicz, J. R., Gratton, E., Laczko, G., Cherek, J., & Limkeman, M. (1984) *Biophys. J. 46*, 463–477.
Lakowicz, J. R., Gryczynski, I., & Cherek, H. (1986a) *J. Biol. Chem. 261*, 2240–2245.
Lakowicz, J. R., Laczko, G., & Gryczynski, I. (1986b) *Rev. Sci. Instrum. 57*, 2499–2506.
Lakowicz, J. R., Cherek, H., Gryczynski, I., Joshi, N., & Johnson, M. L. (1987a) *Biophys. Chem. 28*, 35–50.
Lakowicz, J. R., Johnson, M. L., Wiczk, W., Bhat, A., & Steiner, R. F. (1987b) *Chem. Phys. Lett. 138*, 587–593.
Lakowicz, J. R., Gryczynski, I., & Wiczk, W. (1988) *Biopolymers 27*, 821–830.
Lanzetta, P. A., Alvazez, L. J., Reinsch, P. S., & Candia, D. A. (1979) *Anal. Biochem. 100*, 95–97.
Lowry, D. H., Rosebrough, N. J., Farr, A. L., & Randall, R. J. (1951) *J. Biol. Chem. 193*, 265–275.
Ludi, H., & Hasselbach, W. (1985) *Biochim. Biophys. Acta 821*, 137–141.
Luedtke, R., Owen, C. S., Vanderkooi, J. M., & Karush, F. (1981) *Biochemistry 20*, 2927–2936.
MacLennan, D. H., Brandl, C. J., Korcjak, B., & Green, N. M. (1984) *Nature 316*, 696–700.
Miki, K., Scott, T. L., & Ikemoto, N. (1981) *J. Biol. Chem. 272*, 9382–9385.
Mitchinson, C., Wilderspin, A. F., Trinnaman, B. J., & Green, N. M. (1982) *FEBS Lett. 146*, 87–92.
Murphy, A. J. (1978) *J. Biol. Chem. 253*, 385–389.
Saito, A., Seiler, S., Chu, A., & Fleischer, S. (1984) *J. Cell Biol. 99*, 875–885.
Saito-Nakatsuka, K., Yamashita, T., Kubota, I., & Kawakita, M. (1987) *J. Biochem. (Tokyo) 101*, 365–376.
Scott, T. L. (1985) *J. Biol. Chem. 260*, 14421–14423.
Squier, T. C., & Thomas, D. D. (1988) *J. Biol. Chem. 263*, 9171–9177.
Squier, T. C., Bigelow, D. J., Garcia de Ancos, J., & Inesi, G. (1987) *J. Biol. Chem. 262*, 4748–4754.
Squier, T. C., Bigelow, D. J., & Thomas, D. D. (1988) *J. Biol. Chem. 263*, 9178–9186.
Squier, T. C., Bigelow, D. J., Fernandez-Belda, F., deMeis, L., & Inesi, G. (1990) *J. Biol. Chem. 265*, 13713–13720.
Stokes, D. L., & Green, N. M. (1990) *Biophys. J. 57*, 1–14.
Suzuki, H., Obara, M., Kuwayama, H., & Kanazawa, T. (1987) *J. Biol. Chem. 262*, 15448–15456.
Taylor, K. A., Dux, L., & Martonosi, A. (1984) *J. Mol. Biol. 174*, 193–204.
Thomas, D. D., & Hidalgo, C. (1978) *Proc. Natl. Acad. Sci. U.S.A. 75*, 5488–5492.
Thorley-Lawson, D. A., & Green, N. M. (1977) *Biochem. J. 167*, 739–748.
Wawryznow, A., Bigelow, D. J., Bishop, J. E., & Collins, J. H. (1990) *Biophys. J. 55*, 354a.
Weber, G., & Daniel, E. (1966) *Biochemistry 5*, 1900–1907.
Weber, K., & Osborne, J. (1969) *J. Biol. Chem. 244*, 4406–4412.
Yamada, S., & Ikemoto, N. (1987) *J. Biol. Chem. 253*, 6801–6807.
Yamamoto, T., Yantorno, R. E., & Tonomura, Y. (1984) *J. Biochem. (Tokyo) 95*, 1783–1791.
Yamashita, T., & Kawakita, M. (1987) *J. Biochem. (Tokyo) 101*, 377–385.
Yasuoka-Yabe, K., & Kawakita, M. (1983) *J. Biochem. (Tokyo) 94*, 665–675.
Yoshida, H., & Tonomura, Y. (1976) *J. Biochem. (Tokyo) 79*, 649–654.